ACS APPLIED MATERIALS & INTERFACES

www.acsami.org

Research Article

Dielectrophoretic Characterization of Dynamic Microcapsules and Their Magnetophoretic Manipulation

Tom Elkeles, Sinwook Park, Jörg G. Werner, David A. Weitz, and Gilad Yossifon*

Cite This: *ACS Appl. Mater. Interfaces* 2022, 14, 15765−15773

Read Online

ACCESS | Metrics & More | Article Recommendations | Supporting Information

ABSTRACT: In this work, we present dielectrophoresis (DEP) and *in situ* electrorotation (ROT) characterization of reversibly stimuli-responsive "dynamic" microcapsules that change the physicochemical properties of their shells under varying pH conditions and can encapsulate and release (macro)molecular cargo on demand. Specifically, these capsules are engineered to open (close) their shell under high (low) pH conditions and thus to release (retain) their encapsulated load or to capture and trap (macro)molecular samples from their environment. We show that the steady-state DEP and ROT spectra of these capsules can be modeled using a single-shell model and that the conductivity of their shells is influenced most by the pH. Furthermore, we measured the transient response of the angular velocity of the capsules under rotating electric field conditions, which allows us to directly determine the characteristic time scales of the underlying physical processes. In addition, we demonstrate the magnetic manipulation of microcapsules with embedded magnetic nanoparticles for lab-on-chip tasks such as encapsulation and release at designated locations and the in situ determination of their physicochemical state using on-chip ROT. The insight gained will enable the advanced design and operation of these dynamic drug delivery and smart lab-on-chip transport systems.

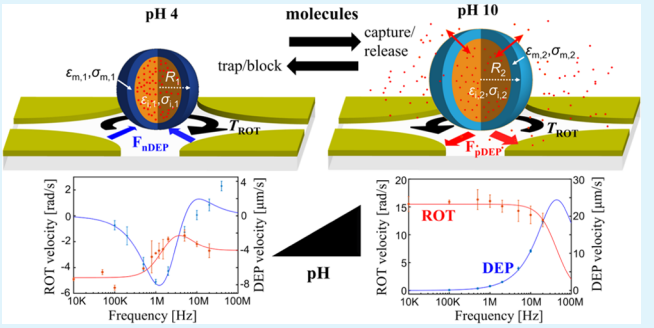

KEYWORDS: *dielectrophoresis, magnetophoresis, microcapsule, microfluidics, stimuli-responsive*

1. INTRODUCTION

Microcapsules are small particles containing a separate core and a shell phase that are of interest for encapsulation, protection, and delivery purposes of a sensitive cargo such as small molecules and biologics, including enzymes, proteins, and nucleic acids.[1−4] In liquid-core microcapsules, the cargo molecule can be suspended in the core under favorable conditions that keep it stable, while it is spatially separated from the shell membrane that controls the release function either through its permeability or an environmental destructive trigger event.[5] Recently, reversibly stimuli-responsive "dynamic" microcapsules have been reported that exhibit a pH-triggered change of the shell's permeability without its destruction, enabling repeated capture, trap, and release of cargo molecules over multiple cycles, as well as staggered on-demand release.[6−9] To gain a fundamental understanding of their response mechanism, an in-depth and direct characterization of the steady-state membrane properties in the permeable and impermeable states, as well as the transient response upon switch of the environmental stimuli, is required. So far, the characterization of the physicochemical state of the shell membrane has been limited to the analysis of their size and permeability using optical and fluorescence microscopy with model probe molecules. Since these methods are indirect probes of the physicochemical properties of the shells, complementary and direct characterization methods are needed to obtain a more complete understanding of the mechanisms and time scales of their reversible response and discover potentially unknown transition states that could impede their application or offer novel ways of their utilization.

Dielectrophoresis (DEP) and electrorotation (ROT) are established techniques used for probing and/or manipulating cells and bioparticles, in which the unique dielectric properties of cells are analyzed using alternating current (AC).[10−22] DEP is defined as the translational motion of neutral particles due to the effects of polarization in a nonuniform electric field. In particular, a crossover frequency (COF) at which the DEP force vanishes, i.e., corresponding to a transition from attraction (positive DEP) to repulsion (negative DEP) and vice versa, can be used as a sensitive discriminator between different cell types or cell conditions and utilized for cell separation and characterization. The asynchronous rotation of particles produced by a rotating electric field (ROT) is an

Received: December 10, 2021
Accepted: March 10, 2022
Published: March 24, 2022

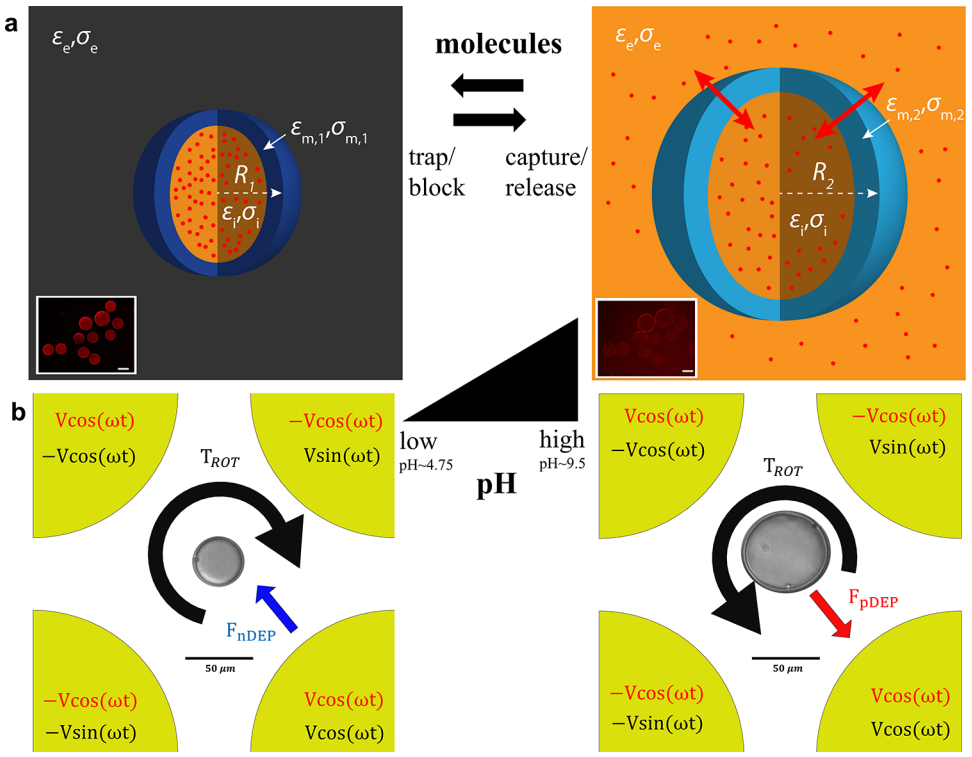

Figure 1. Dielectrophoretic characterization of dynamic poly(acid) microcapsules. (a) Schematic illustrations of the steady-state behavior of the dynamic microcapsules under varying pH in terms of their size and membrane permeability. The insets are confocal microscopy images of poly(acid) microcapsules where fluorescent molecules (TRITC−dextran, 4.4 kDa) are either trapped within it at low pH or are able to transport across the membrane at high pH conditions, respectively. The white scale bar in insets is 50 μm. (b) Representative ROT/DEP response of microcapsules using a quadrupolar electrode array at 1 MHz in low- and high-pH solutions. The black scale bars in part (b) is 50 μm.

additional electrokinetic technique used to determine the dielectric properties of the particles, which also depends on the relative dielectric properties of the capsule and medium and the frequency of the rotational electric field.[15,23−28] The DEP and ROT are governed by the respective real and imaginary parts of the Clausius−Mossotti (CM) factor, which characterizes the relative polarizability of the capsule versus that of the medium. The combination of DEP and ROT spectra with theoretical models enables reliable characterization of the particle's dielectric properties.[29]

Herein, we characterized for the first time, to the best of our knowledge, the dielectric properties of dynamic poly(acid) microcapsules using DEP/ROT techniques, by analyzing the experimental results using a single-shell model. We have further analyzed the transient response of the electrical and geometrical properties of these capsules when introduced to solutions of different pH values. Finally, we have demonstrated the magnetophoretic manipulation of such dynamic microcapsules containing magnetite nanoparticles in their shells within a microfluidic network that can perform different tasks on intaking and releasing drug/sample in between reservoirs in combination with their in situ ROT characterization.

2. RESULTS AND DISCUSSION

2.1. Steady-State DEP and ROT Characterization of Capsules at Various pH. The size and membrane permeability of the dynamic poly(acid) microcapsules vary with the pH of their aqueous environment, as shown in Figure 1a. Specifically, at low pH, the membrane permeability almost vanishes, as shown by the confocal images showing the retention of the fluorescent molecules (TRITC−Dextran, 4.4 kDa) trapped within the capsule over a period of time (1 h). In contrast, at high pH, both the size of the capsule as well as its permeability are significantly increased, thus enabling the transport of the fluorescent molecules across its membrane. Figure 1b schematically shows the observed ROT and DEP response of a poly(acid) capsule under an applied electric field with a frequency of 1 MHz in a low and high pH environment. It is seen that the DEP and ROT response switch directions from negative DEP (nDEP) to positive DEP (pDEP) and from an antifield to a cofield as the pH changes from low-to-high values, respectively.

To determine the dielectric properties of the poly(acid) microcapsules under various pH conditions, we characterized their steady-state DEP and ROT response in four aqueous buffer solutions. Figure 2a shows the observed rotation of the capsules during ROT at different pH values superimposed on the corresponding microscopic images, showing a change in the rotation speed or direction depending on the applied frequency. Based on the ROT torque equation (eq 2), the angular velocity (eq 6) depends quadratically on the applied voltage while its direction depends on the sign of the imaginary parts of the CM factor (eq 3). It is noted that the applied voltage for ROT at three low-pH environments (i.e., deionized (DI) water, pH 4, and pH 7) was 10 V_{pp}, while a lower voltage (5 V_{pp}) was applied in pH 10 because of a strong ROT and pDEP response of the capsules. Figures 2b and S1 summarize the measured angular and linear velocities corresponding to ROT and DEP responses, respectively, along with the fitted single-shell model (Table 1). In this simplest model, the capsule is composed of a spherical membrane that surrounds an inner core, each characterized by its own complex

https://doi.org/10.1021/acsami.1c23482
ACS Appl. Mater. Interfaces 2022, 14, 15765−15773

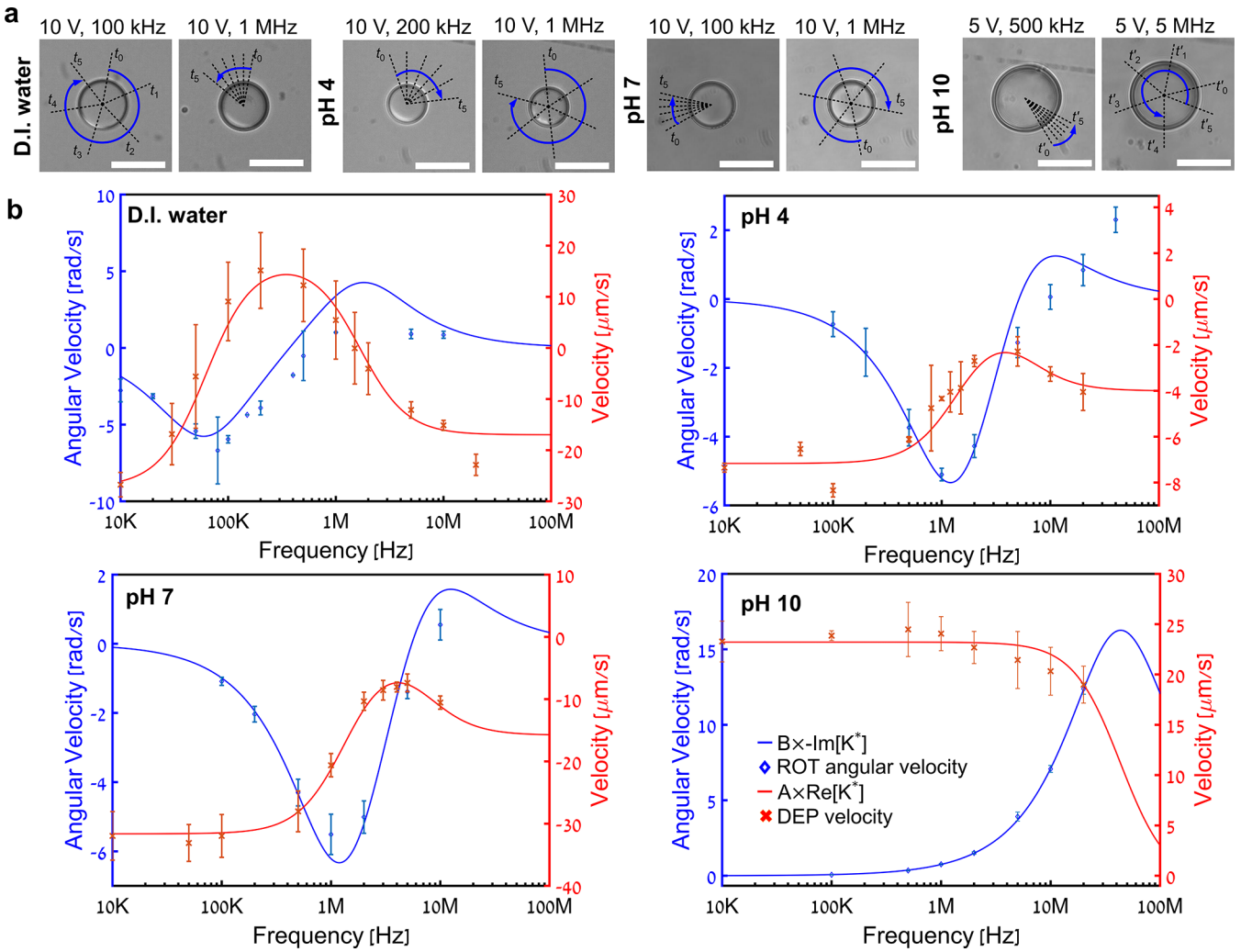

Figure 2. ROT and DEP characterization of the microcapsules in steady-state conditions within various pH environments. (a) Superimposed images showing the representative ROT motion of microcapsules under varying applied frequencies in DI water (~ pH 5.5), sodium acetate buffer (~pH 4.75), phosphate-buffered saline (PBS)(~pH 7), and glycine buffer (pH ~ 9.5). The black dashed lines indicate the change in angular rotations ($\Delta\theta$) within time intervals of 200 ms (i.e., 1 s of the time interval between t_0 and t_5) and 1 s (5 s of the time interval between t_0' and t_5') for the three low-pH environments (DI water, pH 4, and pH 7) and pH 10, respectively. The blue solid arrows indicate the direction of the rotation and the white scale bars are 50 μm. (b) Experimental DEP and ROT spectra of the microcapsule with a theoretical fit under various pH environments corresponding to part (a).

Table 1. Dynamic Capsules DEP and ROT Spectra and a Single-Shell Model Fitting Parameters[a]

	fitted						measured		
solution	$\sigma_{membrane}\left[\frac{mS}{cm}\right]$	$\sigma_{interior}\left[\frac{mS}{cm}\right]$	$\varepsilon_{membrane}$	$\varepsilon_{interior}$	A	B	$\sigma_{electrolyte}\left[\frac{mS}{cm}\right]$	$R_{capsule}$ [μm]	$t_{membrane}$ [μm]
pH4	$9{\cdot}10^{-4}{}^{+2.1{\cdot}10^{-3}}_{-9{\cdot}10^{-4}}$	$0{\cdot}24^{+5{\cdot}10^{-2}}_{-7{\cdot}10^{-2}}$	$24.31^{+9}_{-2.3}$	$32.58^{+11.5}_{-13.5}$	$14.9^{+0.7}_{-1.5}$	$30.4^{+4}_{-5.4}$	$0.2^{\pm0.01}$	$20^{\pm0.1}$	$3^{\pm0.1}$
DI water (pH ~ 5)	$1.9{\cdot}10^{-4}{}^{+6{\cdot}10^{-5}}_{-7{\cdot}10^{-5}}$	$0{\cdot}126^{+16{\cdot}10^{-3}}_{-31{\cdot}10^{-3}}$	$28.2^{+3.1}_{-2.3}$	$41.8^{+7.1}_{-7.4}$	$75.2^{+8}_{-4.5}$	$20.7^{+3.5}_{-2.5}$	$5{\cdot}10^{-3^{\pm10^{-5}}}$	$22^{\pm0.1}$	$3.5^{\pm0.1}$
PBS (pH ~ 7)	$1.1{\cdot}10^{-3}{}^{+9{\cdot}10^{-4}}_{-1.1{\cdot}10^{-3}}$	$0.31^{+0.016}_{-0.02}$	$37.4^{+1.6}_{-3.6}$	$30.8^{+1.5}_{-16.2}$	$65.5^{+4.6}_{-0.9}$	$32^{+3.3}_{-5.2}$	$0.25^{\pm0.01}$	$25^{\pm0.1}$	$4^{\pm0.1}$
pH 10	$18^{+0.3}_{-0.5}$	$0.162^{+0.11}_{-0.16199}$	$44^{+32}_{-33.5}$	$72.6^{+7.4}_{-11.5}$	$26^{+0.4}_{-0.1}$	$35^{+0.8}_{-0.4}$	$0.2^{\pm0.01}$	$35^{\pm0.1}$	$5^{\pm0.1}$

[a]Range of the fitted parameters (left) is obtained from the sensitivity algorithm: it represents the range in which the root mean square (RMS) of the fitting does not change more than 5%. The right side of the table refers to the measured parameters. Their range of the measured values (right) corresponds to the error of the measurement (i.e., the resolution of the microscope, the precision of the conductivity meter, etc.).

permittivity consisting of the real permittivity (ε) and ionic conductivity (σ) (i.e., $\varepsilon_{interior}$ and $\sigma_{interior}$ for the inner core and $\varepsilon_{membrane}$ and $\sigma_{membrane}$ for the membrane). The expression for the CM factor (eqs 3 and 4) includes the complex primitivity of the external electrolyte solution ($\varepsilon_{electrolyte}$, $\sigma_{electrolyte}$), the capsule's radius ($R_{capsule}$), and membrane thickness ($t_{membrane}$).[30,31] Whereas $\sigma_{electrolyte}$, as well as $R_{capsule}$ and $t_{membrane}$ were determined using a conductivity meter (Table 1) and optical microscopy, respectively; the other parameters including the proportionality factors A and B were fitted to the

https://doi.org/10.1021/acsami.1c23482
ACS Appl. Mater. Interfaces 2022, 14, 15765−15773

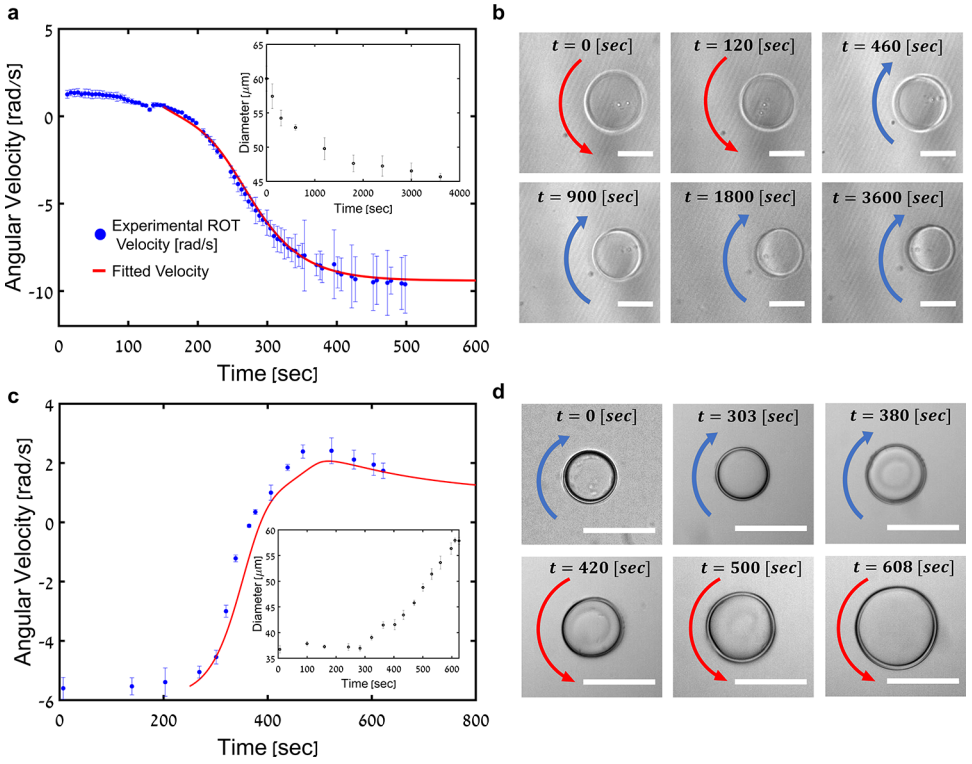

Figure 3. Transient ROT response of dynamic changes of microcapsules by switching pH conditions within a microchamber with embedded quadrupolar electrode arrays. (a) Time-resolved angular ROT velocity (1 MHz, 10 V_{pp}) of a capsule suspended for 1 day in a high-pH (~9.5) solution and introduced into a low-pH (~4.75) solution. (b) Corresponding microscopy images showing the transient response of part (a). (c) Time-resolved angular ROT velocity (1 MHz, 10 V_{pp}) of a capsule that was suspended for 1 day in PBS and introduced to a high-pH (~9.5) solution through diffusion (closed reservoir). (d) Corresponding microscopy images showing the transient response of part (c). Insets of parts (a) and (c) depict the change of the capsule's diameter ($D_{capsule}$) over the same time period. The red and blue arrows in parts (b) and (d) indicate the direction of the cofield and the antifield, respectively, and the white scale bars are 50 μm.

ROT data using a single-shell model. The similarity between the DEP and ROT responses of the capsules in solutions of pH 4 and pH 7 is due to the similar values obtained for the capsule's membrane and interior dielectric properties (Table 1). The high pH 10 case has a distinctly different DEP/ROT behavior due to the change in the membrane conductivity (Table 1, Figure S2). The most sensitive parameter to the change of pH buffer is the conductivity of the membrane ($\sigma_{membrane}$), which varies by orders of magnitude from low-to-very-high values with an increase in pH. This is in correspondence to the physical mechanism of the functional carboxylic acid groups of the membrane, which are expected to deprotonate and become negatively charged at a pH value above their pK_a that, in turn, results in both the enlargement of the capsule size due to water swelling and charge repulsion. This swelling of the shell also leads to an increased permeability of the membrane and higher effective ionic conductivity due to the presence of counterions and increased mesh size. It is noted that the relative permittivity of the interior core, $\varepsilon_{interior}$, seems to depend on the solution pH, and while in a high pH it is (~73) close to that of water (~80), in lower pH solutions, it is smaller (~33 in pH 4). It is suggested that the presence of poly(vinyl alcohol) (PVA) molecules within the interior core due to the fabrication process results in the lowering of the effective solution permittivity, as was confirmed by electrical impedance spectroscopy (EIS) measurements (see Table S2 and Figure S3 for more details).

2.2. Transient ROT Response of Capsules. In addition to the steady-state response, it is important to examine the transient response of the dynamic capsules so as to further understand the underlying processes and their time scales. Such a transient response due to a sudden change of the solution pH is shown in Figure 3 in terms of both the time-varying ROT angular velocity with a fixed frequency (1 MHz, 10 V_{pp}) as well as the change in the radius of the capsule (insets of parts (a) and (c)). The capsules were then suspended for 1 day in either a high-pH (~9.5) or a PBS (pH ~ 7) buffer before their introduction into a low-pH (~4.75) and a high-pH (~9.5) buffer, respectively. The initial times (t = 0 s) in Figure 3a,c correspond to the approximate time when the capsule started to respond to the change of the solutions' pH. In the case of high to low pH (Figure 3a,b), the capsule (contained within a small volume of a high-pH buffer, ~9.5) was dropped into a low-pH (~4.75) solution of a much larger volume, while in the low-to-high pH case (Figure 3c), a high-pH (~9.5) solution was introduced and diffused into the chamber already containing the capsule within a pH ~ 7 buffer. It is clearly shown how the ROT velocity switches direction simultaneously to the change in the capsule size. For example, the large-size capsule ($R_{capsule}$ ~ 35 μm) equilibrated in a high pH solution transiently changed its rotating direction simultaneously to its size reduction (Figure 3a,b). The switching of the direction of the angular velocity is due to the significant change in the membrane conductivity upon changing the solution pH, as was explained in the previous section. The experimental transient ROT responses were fitted using a semiempirical model that is described in Section 4.7. In both cases of solution's pH change, the semiempirical value

https://doi.org/10.1021/acsami.1c23482
ACS Appl. Mater. Interfaces 2022, 14, 15765−15773

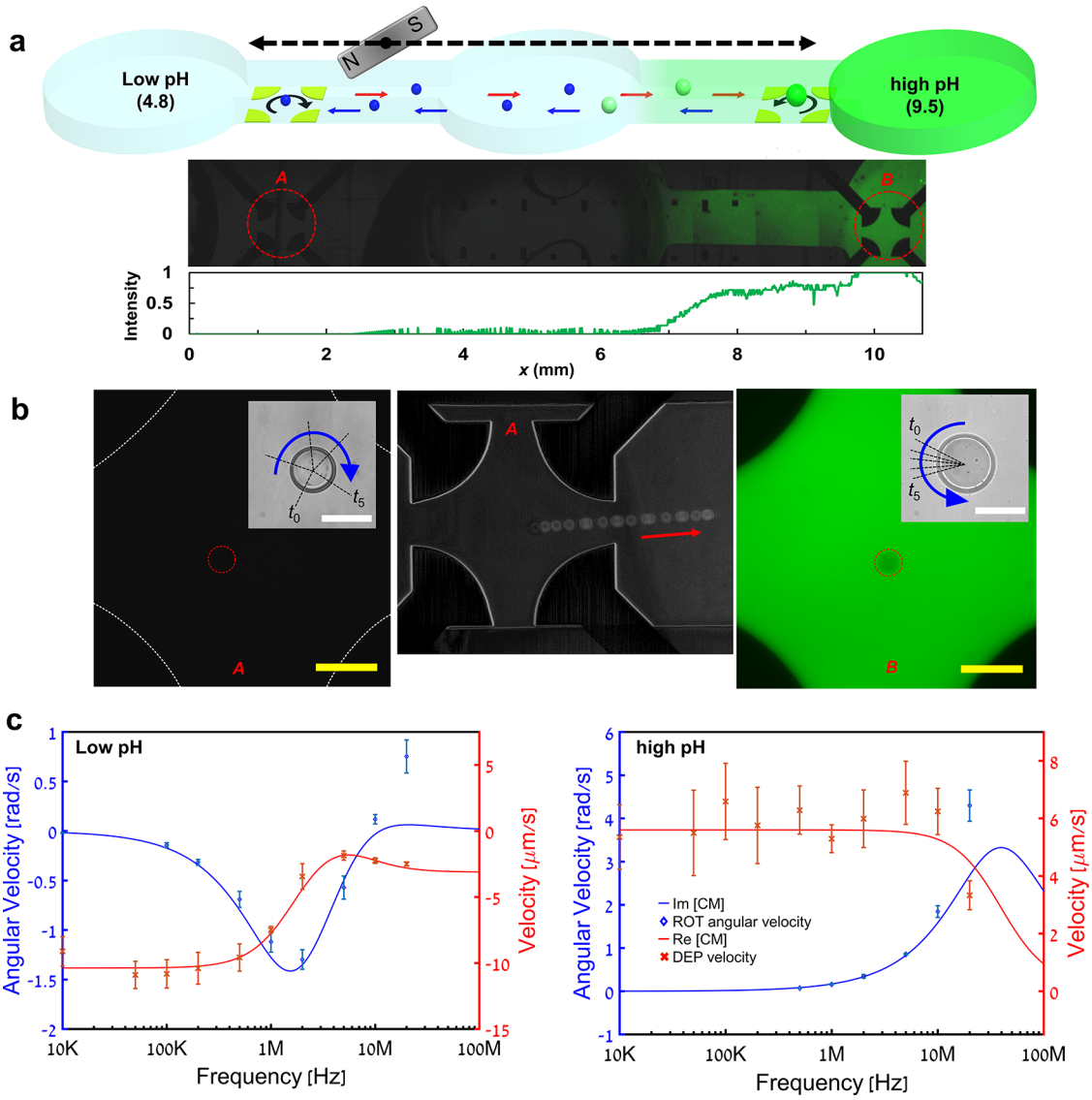

Figure 4. Transport of magnetic microcapsules and dynamic ROT characterization within a microfluidic channel exhibiting a gradient in pH and containing embedded quadrupolar electrode arrays. (a) Schematic illustration of the dynamic changes of the magnetic microcapsules during their magnetic transport between different pH environments with their ROT direction at 1 MHz (top) and a superimposed microscopic bright-field and fluorescent image of the channel (middle). The corresponding normalized fluorescent intensity profile (bottom) was set by a pH 4.8 solution without fluorescent molecules (FITC−Dextran) and a pH 9.5 solution with fluorescent molecules as 0 and 1, respectively; (b) microscopic images of the capsules in locations A and B and the superimposed time-lapse image showing magnetophoretic transport of microcapsules, where A and B correspond to the center of the quadrupolar electrode array in the vicinity of the low- and high-pH reservoirs, respectively. The inset superimposed images represent the ROT motion of microcapsules extracted from movie S4. The white and yellow scale bars are 50 and 100 μm, respectively. (c) Steady-state ROT and DEP spectra of the magnetic capsules along with the theoretical fitted models (Table S1 in supporting materials) for low- and high-pH buffers. The blue and red points and lines represent experimental data with the fitted model for ROT and DEP responses, respectively.

was taken after some time ∼150−250 s to avoid the short-time processes of the buffer exchange, i.e., either the physical introduction of the capsule into the low-pH solution or the diffusion process of the high-pH solution into the chamber already containing the capsule within a low-pH buffer. Interestingly, while the ROT angular velocity approaches steady-state values within ∼500−600 s in both abrupt changes of the solution to either low- or high-pH values, the change of the radius from a large value at high pH to a small value at low pH is significantly more prolonged than the reversed change, i.e., enlargement of the radius when shifted from low-to-high pH. Such a difference in response time is in accordance with the previously observed behavior for these dynamic capsules where permeability ceased within seconds upon lowering of the pH, while the decrease in capsule size takes minutes to hours to occur.[6] It is hypothesized that the long response time in capsule size is due to the significantly hindered and slow egress of water from the core through the shell at low pH conditions.

2.3. On-Chip Manipulation and In Situ Characterization of Magnetic Dynamic Capsules. We examined the potential use of such dynamic microcapsules for lab-on-chip operations such as trap, transport, and release of captured molecules for targeted delivery applications wherein the permeability of the membrane responds to the local pH values of the solution. For this purpose, we fabricated capsules with

https://doi.org/10.1021/acsami.1c23482
ACS Appl. Mater. Interfaces 2022, 14, 15765−15773

embedded magnetic nanoparticles, which could then be manipulated magnetophoretically *via* an external magnet.[32] Prior to performing on-chip tasks of the magnetic capsules, their steady-state ROT and DEP responses were characterized, using the same experimental setup as in Figure 2. A clear distinct ROT and DEP frequency response of the magnetic capsules for low and high pH (i.e., direction switches from an antifield to a cofield and from nDEP to pDEP) were obtained at 1 MHz, which is similar to those of the nonmagnetic capsules, as shown in Figure 4c and Supporting Information Table S1. Thus, the magnetic nanoparticles do not strongly affect the dielectric response (i.e., CM factor) of the magnetic capsule, which similarly to the nonmagnetic capsule is dominated by its response to the change of pH.

Magnetophoretic manipulation of the capsules containing magnetic nanoparticles enables their controlled movement on microfluidic chips to perform localized tasks, while in situ characterization of the capsules using ROT allows for the direct determination of their physicochemical state. We demonstrate these concepts within a microfluidic channel by moving the microcapsules back and forth between two reservoirs of high and low pH, respectively, each containing ROT electrodes and with a target molecule present on the high-pH side (see Figure 4a). The target molecule for this demonstration was 0.2 mg mL^{-1} fluorescein isothiocyanate−dextran (FITC−Dextran, 4.0 KDa), and its concentration gradient is clearly shown in the microscopic fluorescence image of Figure 4a. Movie S4 shows the controlled movement of the magnetic and dynamic microcapsules from the low-pH to the high-pH area of a microfluidic channel and the distinct ROT response of the capsules in these respective areas. The microscopic images of the capsules in locations A and B, corresponding to the center of the quadrupolar electrode array in the vicinity of the low- and high-pH reservoirs, respectively, are shown in Figure 4b. The corresponding in situ ROT response (1 MHz, 10 V_{pp}) of the magnetic capsules for the low- and high-pH conditions are in agreement with those at steady state. It is noted that the external magnet is not present during the ROT tests so as to decouple any possible external magnetic force and the electrical ROT response. Additionally, the capsules show the uptake of the target molecule at high pH (Figure 4b).

3. CONCLUSIONS

Herein, we demonstrated the DEP and ROT response of dynamic microcapsules to varying pH values of the buffer in both steady state and transient conditions. We show that the membrane conductivity is the most sensitive parameter of the capsules' dielectric properties and increases by orders of magnitude when the capsule transitions from low-to-high pH values. This is in correspondence to the expected charging of the tethered acid groups in the shell membrane at high pH values, which leads to both enlargement of the capsule, increased shell permeability, and high ion concentration in the shell. The transient response, obtained via *in situ* ROT characterization, also showed the characteristic time of these changes and revealed a large difference between the very fast change of the charging of the membrane compared to the change in capsule size. Finally, we demonstrated the applicability of this dynamic capsule for on-chip operations such as capture and transport of target molecules that are controlled by an external magnetic field with simultaneous characterization, which can be used for various purposes such as targeted or single-cell drug delivery for in vitro studies or sampling of molecules in specified local environments for further analysis and more.

4. METHODS

4.1. Device Fabrication. The quadrupolar electrode array substrate (Figure 1) was fabricated using photolithography and wet-etching processes to have distances across the center of electrodes of 100 μm for DEP and 500 μm for ROT characterization as previously described.[29] Layers of Au/Cr (200/30 nm in thickness) were evaporated onto a glass substrate. After the electrode array was fabricated, a flexible silicon chamber of 1 mm in both diameter and depth (Grace BioLabs) was attached onto the electrode substrate. For magnetic manipulation of capsules, a polydimethylsiloxane (PDMS)-based microfluidic layer (1 mm in thickness) was assembled on the glass substrate with the embedded quadrupolar ROT electrode arrays (Figure 4).[33]

The PDMS layer, fabricated using standard soft lithography and the PDMS replica mold technique, consists of three microchambers (5 mm in diameter, 30 μm in height) with holes and the connecting microchannels (2 mm in width, 30 μm in height). Above the holes in each microchamber, an additional silicone reservoir (1 mm in height, 5 mm in diameter) was attached to fill the solution, which prevents evaporation of solution within the microchamber and controls the possible flow within the microfluidic chamber during experiments.

4.2. Fabrication of Capsules. *4.2.1. Chemicals and Materials.* 4-Pentenoic anhydride (PenAn), tri(ethylene glycol) divinyl ether (TEGDVE), pentaerythritol tetrakis(3-mercaptopropionate) (PETMP), poly(vinyl alcohol) (M_w 13 000−23 000, 98% hydrolyzed, PVA), iron(II,III) oxide nanopowder (50−100 nm particle size from SEM), and the photoinitiator 2-hydroxy-2-methylpropiophenone (Darocure 1173) were purchased from Sigma-Aldrich and used as received. Phosphate-buffered saline (PBS, 10X, RNase free) was purchased from Alfa Aesar and diluted by DI water to 1X before use.

4.2.2. Fabrication of Microfluidic Drop-Making Devices. The water-in-oil-in-water (W/O/W) double-emulsion drops were fabricated using polydimethylsiloxane (PDMS) microfluidic drop makers obtained from soft lithography, as previously described.[34] Briefly, the PDMS devices comprise two consecutive flow-focusing junctions with different channel widths and heights. The channels of the first junction have a depth of 50 μm and a width of 40 μm, while the channels crossing and exiting the second junction have a depth of 150 μm and a width of 50 or 100 μm. The PDMS devices are plasma-bonded and placed in a vacuum for 1 week before use to achieve the native hydrophobicity of PDMS after the bonding procedure. No additional surface treatment is applied for the PDMS devices.

4.2.3. Synthesis of Double-Emulsion Microcapsules. Microcapsules were templated by double-emulsion drops fabricated with microfluidic drop-making devices, as described previously.[6,34] The inner aqueous core phase contained 2 wt % PVA in 1X PBS buffer, the middle oil phase was a mixture of the liquid monomers PenAn/TEGDVE/PETMP/photoinitiator at a molar ratio of 1:1.64:2.64:0.11, and the outer aqueous phase contained 9 wt % PVA in 1X PBS buffer. For magnetic microcapsules, 0.2 wt % magnetic iron(III) oxide nanopowder was dispersed in the monomer mixture at 4 °C immediately before drop making. The flow rates for the inner, middle, and outer phases (I−M−O) were controlled by Harvard Apparatus syringe pumps to be at 8000−150−450 μL h^{-1} and at 8000−300−600 μL h^{-1} for nonmagnetic and magnetic microcapsules, respectively. Following double-emulsion formation, the drops flow through a short collection tube into a collection bath of 1X PBS buffer and are immediately irradiated with UV light (OmiCure S1500, 320−500 nm filter) to photopolymerize the shells. The double-emulsion drops are stable toward coalescence and collapse between microfluidic formation and UV-induced solidification. The microcapsules were collected and washed with 1X PBS buffer five times through successive replacement of the supernatant with fresh PBS buffer, followed by centrifugation at 2000*g*. The size distribution of the fabricated microcapsules under various pH

https://doi.org/10.1021/acsami.1c23482
ACS Appl. Mater. Interfaces 2022, 14, 15765−15773

conditions is described in Figure S4. The thus-obtained poly(anhydride) microcapsules were hydrolyzed to reversibly pH-responsive (dynamic) poly(acid) microcapsules in 1X PBS at room temperature for 3 days.

4.3. Experimental Setup for Capsule Characterization by DEP/ROT. Figure 1 shows the quadrupolar electrode array experimental setup for steady-state DEP and ROT characterization of the capsules. A total of 5−10 μL of a solution comprised of capsules suspended within various solutions were inserted into an open chamber filled with various pH solutions. We used appropriate ratios of acetic acid and sodium hydroxide for pH 4.5, phosphate-buffered saline (PBS) for pH 7, and glycine for pH 9.5, and their conductivities are described in Table 1. Prior to the introduction of capsules, the surface of the electrode array was wet in DI water with Tween 20 (0.1% w/w) to prevent the absorption of capsules for 10 min and washed with target solutions. The conductivities of all buffer solutions were measured using a portable conductivity meter (LAQUAtwin, Horiba). During all DEP experiments, one or a few capsules were placed within the electrode array to prevent capsule-to-capsule electrical interaction. Various AC field frequencies with a sinusoidal waveform were applied using a function generator (33250A, Agilent). To minimize the side effects (e.g., electrolysis, joule heating, or electroporation[35]) of the electric field, a sufficiently low-amplitude AC field (5 V_{pp}−10 V_{pp}) that still provides a sensible DEP effect was applied. To generate the rotating field (10 V_{pp}), a four-channel arbitrary waveform generator (TGA12104, TTI) with a 90° phase-shift between the channels was connected to four planar electrodes. The motion of the capsules, either linear translation due to DEP or rotational motion due to ROT, was recorded using an Andor Neo sCMOS camera attached to a Nikon TI inverted epi-fluorescent microscope with a 20× objective lens and further analyzed by a particle tracking method using image processing software (ImageJ). Data shown in all results are the averaged values from four to five capsules. We modeled the data points using a single-shell model to extract the fitting parameters with optimization using MATLAB. To fit the single-shell model to the experimental data, we used a least-squares-based Matlab function that finds a local minimum of the root mean square (RMS) of the fitting. To achieve a range for each parameter, a sensitivity algorithm calculated the range of each parameter in which the RMS of the fitting does not change more than 5%.

4.4. Transient ROT Characterization of Capsules. For the transient experiments, different techniques were used for capturing the transient reaction of the dynamic capsules. To demonstrate the encapsulation process, capsules that were immersed for 1 day in a high-pH solution were introduced into an open reservoir that contains a low-pH solution. On the other hand, to demonstrate the intake process, capsules that were immersed for 1 day in a low-pH solution were introduced into a closed reservoir (9 mm in diameter, 0.11 mm in thickness) that contains the low-pH solution. After the capsules were placed inside the electrode array, a pipette was used to diffuse the high-pH solution with fluorescent molecules (FITC−Dextran) into the chamber, up until the pH inside was high enough to start affecting the capsule.

4.5. Magnetophoretic Manipulations of Magnetic Capsules. Two distinct low- and high-pH environments were formed at the ends (left and right) of reservoirs of the fabricated platform, respectively, and the magnetic capsules placed in the reservoir were magnetophoretically transported using external permanents (neodymium, 20 × 25 × 10 mm^3, 53 of (BH)ax/MGOe). Prior to establishing the final pH environment, the channel was filled with a low-pH solution without magnetic capsules. Then, a high-pH solution with fluorescent molecules (FITC−dextran 4.0 kDa) replaced the right end reservoir. The middle chamber filled with a low-pH solution prevents the propagation of the high-pH solution toward the left reservoir as a flow-compensated chamber (Figure 4a) during solution replacement. Then, 3 μL of a solution comprised of capsules was introduced into the left end microchambers and transported onto the left ROT electrode array. During the transport of magnetic capsules back and forth between different pH reservoirs, pH gradients were continuously monitored by switching fluorescent and bright-field modes. During the ROT characterization of the capsule at different locations, we used the bright-field mode to observe the shape of the capsule membrane.

4.6. Single-Shell Model of the DEP and ROT Response. Given a nonuniform electric field, the time-averaged DEP force for a lossy dielectric spherical particle suspended within a lossy dielectric medium is given as follows[30]

$$F_{DEP} = \pi\varepsilon_e R^3 Re[K^*]\nabla|E|^2 \tag{1}$$

where $R_{capsule}$ is the outer radius of the capsule, E is the amplitude of the electric field, ε_e is the permittivity of the electrolyte, and Re (K^*) is the real part of the CM factor. In the case of a rotating (ROT) electric field, the time-averaged torque exerted on the capsule is related to the imaginary part of the CM factor[30,36]

$$T_{ROT} = -4\pi\varepsilon_e R^3 Im[K^*]E^2\vec{z} \tag{2}$$

where $\vec{z}$ is a unit vector normal to the electrode's surface and Im(K^*) is the imaginary part of the CM factor. The CM factor is a complex term dependent on angular frequency (ω) of the applied electric field and the dielectric properties of the given capsule and medium

$$K^*(\omega) = \frac{\varepsilon^*_{capsule} - \varepsilon^*_{electrolyte}}{\varepsilon^*_{capsule} + 2\varepsilon^*_{electrolyte}},\ \varepsilon^* = \varepsilon + \frac{\sigma}{j\omega} \tag{3}$$

where $\varepsilon^*_{capsule}$ and $\varepsilon^*_{electrolyte}$ are the complex permittivities of the capsule and the electrolyte, respectively, and ε and σ are the real permittivity and the conductivity, respectively.

The capsule is modeled as a single-shell with a uniform inner core ($\varepsilon_{interior}$, $\sigma_{interior}$) and a thin spherical wall ($\varepsilon_{membrane}$, $\sigma_{membrane}$) of thickness $t_{membrane}$. The expression for the effective complex permittivity of the capsule, $\varepsilon^*_{capsule}$, for the single-shell model is

$$\varepsilon^*_{capsule} = \varepsilon^*_{membrane}\left[\left(\frac{R}{R-t}\right)^3 + 2\left(\frac{\varepsilon^*_{interior} - \varepsilon^*_{membrane}}{\varepsilon^*_{interior} + 2\varepsilon^*_{membrane}}\right) \Big/ \left(\frac{R}{R-t}\right)^3 - \left(\frac{\varepsilon^*_{interior} - \varepsilon^*_{membrane}}{\varepsilon^*_{interior} + 2\varepsilon^*_{membrane}}\right)\right] \tag{4}$$

For simplicity, it is assumed that the DEP force and the ROT torque are balanced by viscous stresses such that the respective DEP velocity ($U_{capsule}$) and ROT angular velocity ($\Omega_{capsule}$) are expressed as[31,37,38]

$$U_{capsule} = A\cdot Re[K^*],\ \text{where}\ A = \frac{\varepsilon_e R^2\nabla|E|^2}{6\eta} \tag{5}$$

$$\Omega_{capsule} = -B\cdot Im[K^*],\ \text{where}\ B = \frac{\varepsilon_e E^2}{2\eta} \tag{6}$$

where A and B are the proportionality factors to be fitted to the experimental data and η is the dynamic viscosity of the electrolyte.

4.7. Semiempirical Model for the Transient Response. The model shown in Figure 3a,c that is fitted to the experimental measurements is assuming, for simplicity reasons, that the only parameter that varies with time upon an abrupt change in the pH conditions is the conductivity of the membrane. Upon a change from low-to-high pH, we assumed the following model

$$\sigma_{intake}(t) = \begin{cases} \sigma_{pH4} e^{t-t_0/\tau_1} & t_0 < t < t_1 \\ \sigma_{pH10} - (\sigma_{pH10} - \sigma_{pH4} e^{t_1-t_0/\tau_1}) e^{-t-t_1/\tau_2} & t_1 < t' \end{cases} \tag{7}$$

where $\sigma_{pH10} = 18e^{-1}$ [S/m] and $\sigma_{pH4} = 9e^{-5}$ [S/m]. The assumption of exponential dependency on time stems from the expected diffusion problem that underlies the change in the membrane properties when the outer solution of a different pH propagates into the membrane from the outside. Here, the fitted time parameters are $t_0 = 250$ [s]; $t_1 = 500$ [s]; $\tau_1 = 35$ [s]; and $\tau_2 = 550$ [s]. For the case of a change from high to low pH, we used the following fitting

https://doi.org/10.1021/acsami.1c23482
ACS Appl. Mater. Interfaces 2022, 14, 15765−15773

$$\sigma_{encapsulation}(t) = \sigma_{pH4} - (\sigma_{pH10} - \sigma_{pH4})e^{-t-t_1/\tau} \quad (8)$$

where the fitted time parameters are τ = 50 [s] and t_1 = 70 [s].

ASSOCIATED CONTENT

Supporting Information

The Supporting Information is available free of charge at https://pubs.acs.org/doi/10.1021/acsami.1c23482.

(Table S1) single-shell model fitting parameters of the magnetic dynamic capsules, (Table S2) fitted parameters for the equivalent circuit of EIS data, (Figure S1) Figure 2 with the same *y*-axis ranges, (Figure S2) parametric analysis of theoretical Re(CM), (Figure S3) Nyquist plot of the measured impedance for various concentrations of the KCl, and additional information on the experimental setup for EIS measurements and additional Supporting Information movies (PDF)

Movie 1: Transient ROT response of a dynamic capsule from low to high pH, showing that when the angular velocity of the capsule changes its direction, the release of the encapsulated interior solution (pH 4.75 without dextran) and the diffusion of the outer solution (pH 9.5 with dextran) into the capsule occurs simultaneously (MP4)

Movie 2: Transient ROT response of a dynamic capsule from low pH (∼4.75) to high pH (∼9.5) with a clear change of the direction of rotation (MP4)

Movie 3: Transient ROT response of a dynamic capsule from high pH (∼9.5) to low pH (∼4.75) with a clear change of the direction of rotation (MP4)

Movie 4: On-chip manipulation of magnetic dynamic capsules back and forth between the high- and low-pH reservoirs including in situ ROT characterizations (MP4)

AUTHOR INFORMATION

Corresponding Author

Gilad Yossifon − *Faculty of Mechanical Engineering, Technion-Israel Institute of Technology, Haifa 3200003, Israel*; orcid.org/0000-0001-7999-2919; Email: yossifon@technion.ac.il

Authors

Tom Elkeles − *Faculty of Mechanical Engineering, Technion-Israel Institute of Technology, Haifa 3200003, Israel*

Sinwook Park − *Faculty of Mechanical Engineering, Technion-Israel Institute of Technology, Haifa 3200003, Israel*

Jörg G. Werner − *John A. Paulson School of Engineering and Applied Sciences, Harvard University, Cambridge, Massachusetts 02138, United States; Department of Mechanical Engineering, Boston University, Boston, Massachusetts 02215, United States*; orcid.org/0000-0001-7845-086X

David A. Weitz − *John A. Paulson School of Engineering and Applied Sciences, Harvard University, Cambridge, Massachusetts 02138, United States*; orcid.org/0000-0001-6678-5208

Complete contact information is available at: https://pubs.acs.org/10.1021/acsami.1c23482

Notes

The authors declare no competing financial interest.

ACKNOWLEDGMENTS

G.Y. acknowledges support from the Israel Science Foundation (ISF) (1938/16). The fabrication of the chip was made possible through the financial and technical support of the Russell Berrie Nanotechnology Institute and the Micro-Nano Fabrication Unit.

REFERENCES

(1) Li, W.; Zhang, L.; Ge, X.; Xu, B.; Zhang, W.; Qu, L.; Choi, C. H.; Xu, J.; Zhang, A.; Lee, H.; Weitz, D. A. Microfluidic Fabrication of Microparticles for Biomedical Applications. *Chem. Soc. Rev.* **2018**, *47*, 5646−5683.

(2) Lee, T. Y.; Choi, T. M.; Shim, T. S.; Frijns, R. A. M.; Kim, S. H. Microfluidic Production of Multiple Emulsions and Functional Microcapsules. *Lab Chip* **2016**, *16*, 3415−3440.

(3) Zhang, W.; Abbaspourrad, A.; Chen, D.; Campbell, E.; Zhao, H.; Li, Y.; Li, Q.; Weitz, D. A. Osmotic Pressure Triggered Rapid Release of Encapsulated Enzymes with Enhanced Activity. *Adv. Funct. Mater.* **2017**, *27*, No. 1700975.

(4) Steinacher, M.; Cont, A.; Du, H.; Persat, A.; Amstad, E. Monodisperse Selectively Permeable Hydrogel Capsules Made from Single Emulsion Drops. *ACS Appl. Mater. Interfaces* **2021**, *13*, 15601−15609.

(5) Brun-Graeppi, A. K. A. S.; Richard, C.; Bessodes, M.; Scherman, D.; Merten, O. W. Cell Microcarriers and Microcapsules of Stimuli-Responsive Polymers. *J. Control. Release* **2011**, *149*, 209−224.

(6) Werner, J. G.; Deveney, B. T.; Nawar, S.; Weitz, D. A. Dynamic Microcapsules with Rapid and Reversible Permeability Switching. *Adv. Funct. Mater.* **2018**, *28*, No. 1803385.

(7) Werner, J. G.; Nawar, S.; Solovev, A. A.; Weitz, D. A. Hydrogel Microcapsules with Dynamic PH-Responsive Properties from Methacrylic Anhydride. *Macromolecules* **2018**, *51*, 5798−5805.

(8) Zhu, H.; Nawar, S.; Werner, J. G.; Liu, J.; Huang, G.; Mei, Y.; Weitz, D. A.; Solovev, A. A. Hydrogel Micromotors with Catalyst-Containing Liquid Core and Shell. *J. Phys. Condens. Matter* **2019**, *31*, No. 214004.

(9) Liu, J.; Chen, H.; Shi, X.; Nawar, S.; Werner, J. G.; Huang, G.; Ye, M.; Weitz, D. A.; Solovev, A. A.; Mei, Y. Hydrogel Microcapsules with Photocatalytic Nanoparticles for Removal of Organic Pollutants. *Environ. Sci.: Nano* **2020**, *7*, 656−664.

(10) Chan, K. L.; Gascoyne, P. R.; Becker, F. F.; Pethig, R. Electrorotation of Liposomes: Verification of Dielectric Multi-Shell Model for Cells. *Biochim. Biophys. Acta, Lipids Lipid Metab.* **1997**, *1349*, 182−196.

(11) Pethig, R. Dielectrophoresis: Status of the Theory, Technology, and Applications. *Biomicrofluidics* **2010**, *4*, No. 022811.

(12) Hanke, C.; Dittrich, P. S.; Reyes, D. R. Dielectrophoretic Cell Capture on Polyester Membranes. *ACS Appl. Mater. Interfaces* **2012**, *4*, 1878−1882.

(13) Zhao, K.; Li, D. Tunable Droplet Manipulation and Characterization by Ac-DEP. *ACS Appl. Mater. Interfaces* **2018**, *10*, 36572−36581.

(14) Zhou, T.; Chen, J.; Kropp, E.; Kulinsky, L. Guided Electrokinetic Assembly of Polystyrene Microbeads onto Photo-patterned Carbon Electrode Arrays. *ACS Appl. Mater. Interfaces* **2020**, *12*, 35647−35656.

(15) Gascoyne, P.; Pethig, R.; Satayavivad, J.; Becker, F. F.; Ruchirawat, M. Dielectrophoretic Detection of Changes in Erythrocyte Membranes Following Malarial Infection. *Biochim. Biophys. Acta, Biomembr.* **1997**, *1323*, 240−252.

(16) Pethig, R. Dielectrophoresis: An Assessment of Its Potential to Aid the Research and Practice of Drug Discovery and Delivery. *Adv. Drug Delivery Rev.* **2013**, *65*, 1589−1599.

(17) Voldman, J. Electrical Forces for Microscale Cell Manipulation. *Annu. Rev. Biomed. Eng.* **2006**, *8*, 425−454.

(18) Pethig, R.; Lee, R. S.; Talary, M. S. Cell Physiometry Tools Based on Dielectrophoresis. *JALA* **2004**, *9*, 324−330.

(19) Hölzel, R.; Pethig, R. Protein Dielectrophoresis: Key Dielectric Parameters and Evolving Theory. *Electrophoresis* **2020**, *42*, 513−538.
(20) Sancho, M.; Martínez, G.; Martín, C. Accurate Dielectric Modelling of Shelled Particles and Cells. *J. Electrostat.* **2003**, *57*, 143−156.
(21) Pethig, R. Review—Where Is Dielectrophoresis (DEP) Going? *J. Electrochem. Soc.* **2017**, *164*, B3049−B3055.
(22) Rozitsky, L.; Fine, A.; Dado, D.; Nussbaum-Ben-Shaul, S.; Levenberg, S.; Yossifon, G. Quantifying Continuous-Flow Dielectrophoretic Trapping of Cells and Micro-Particles on Micro-Electrode Array. *Biomed. Microdevices* **2013**, *15*, 859−865.
(23) Wang, X. B.; Huang, Y.; Gascoyne, P. R. C.; Becker, F. F.; Hölzel, R.; Pethig, R. Changes in Friend Murine Erythroleukaemia Cell Membranes during Induced Differentiation Determined by Electrorotation. *BBA, Biomembr.* **1994**, *1193*, 330−344.
(24) Yang, J.; Huang, Y.; Wang, X.; Wang, X. B.; Becker, F. F.; Gascoyne, P. R. C. Dielectric Properties of Human Leukocyte Subpopulations Determined by Electrorotation as a Cell Separation Criterion. *Biophys. J.* **1999**, *76*, 3307−3314.
(25) Jones, T. B. Liquid Dielectrophoresis on the Microscale. *J. Electrostat.* **2001**, *51*−*52*, 290−299.
(26) García-Sánchez, P.; Ren, Y.; Arcenegui, J. J.; Morgan, H.; Ramos, A. Alternating Current Electrokinetic Properties of Gold-Coated Microspheres. *Langmuir* **2012**, *28*, 13861−13870.
(27) Lo, Y. J.; Lei, U.; Chen, K. Y.; Lin, Y. Y.; Huang, C. C.; Wu, M. S.; Yang, P. C. Derivation of the Cell Dielectric Properties Based on Clausius-Mossotti Factor. *Appl. Phys. Lett.* **2014**, *104*, No. 113702.
(28) Lei, U.; Sun, P. H.; Pethig, R. Refinement of the Theory for Extracting Cell Dielectric Properties from Dielectrophoresis and Electrorotation Experiments. *Biomicrofluidics* **2011**, *5*, No. 044109.
(29) Park, S.; Capelin, D.; Piriatinskiy, G.; Lotan, T.; Yossifon, G. Dielectrophoretic Characterization and Isolation of Jellyfish Stinging Capsules. *Electrophoresis* **2017**, *38*, 1996−2003.
(30) Morgan, H.; Green, N. G. *AC Electrokinetics: Colloids and Nanoparticles*, 2003, DOI: 10.1109/EMR.2017.2734298.
(31) Gagnon, Z. R. Cellular Dielectrophoresis: Applications to the Characterization, Manipulation, Separation and Patterning of Cells. *Electrophoresis* **2011**, *32*, 2466−2487.
(32) Huang, G.; Li, M.; Yang, Q.; Li, Y.; Liu, H.; Yang, H.; Xu, F. Magnetically Actuated Droplet Manipulation and Its Potential Biomedical Applications. *ACS Appl. Mater. Interfaces* **2017**, *9*, 1155−1166.
(33) Park, S.; Yossifon, G. Micromotor-Based Biosensing Using Directed Transport of Functionalized Beads. *ACS Sens.* **2020**, *5*, 936−942.
(34) Romanowsky, M. B.; Abate, A. R.; Rotem, A.; Holtze, C.; Weitz, D. A. High Throughput Production of Single Core Double Emulsions in a Parallelized Microfluidic Device. *Lab Chip* **2012**, *12*, 802−807.
(35) Castellanos, A.; Ramos, A.; González, A.; Green, N. G.; Morgan, H. Electrohydrodynamics and Dielectrophoresis in Microsystems: Scaling Laws. *J. Phys. D. Appl. Phys.* **2003**, *36*, 2584−2597.
(36) Jones, T. B. *Electromechanics of Particles*, 2005, DOI: 10.1016/S0032-5910(97)82724-6.
(37) Honegger, T.; Berton, K.; Picard, E.; Peyrade, D. Determination of Clausius-Mossotti Factors and Surface Capacitances for Colloidal Particles. *Appl. Phys. Lett.* **2011**, *98*, No. 181906.
(38) Sancho, M.; Martínez, G.; Muñoz, S.; Sebastián, J. L.; Pethig, R. Interaction between Cells in Dielectrophoresis and Electrorotation Experiments. *Biomicrofluidics* **2010**, *4*, No. 022802.

https://doi.org/10.1021/acsami.1c23482
ACS Appl. Mater. Interfaces 2022, 14, 15765−15773